frontiers in Earth Science

ORIGINAL RESEARCH
published: 02 September 2020
doi: 10.3389/feart.2020.574206

Temperature Variation on the Central Tibetan Plateau Revealed by Glycerol Dialkyl Glycerol Tetraethers From the Sediment Record of Lake Linggo Co Since the Last Deglaciation

Yue He[1,2], Juzhi Hou[3,4,5], Mingda Wang[6], Xiumei Li[7], Jie Liang[3], Shuyun Xie[5] and Yurong Jin[1]*

[1]School of Resources, Hebei GEO University, Shijiazhuang, China, [2]Key Laboratory of Regional Geology and Mineralization, Hebei GEO University, Shijiazhuang, China, [3]Key Laboratory of Alpine Ecology, Institute of Tibetan Plateau Research, Chinese Academy of Sciences, Beijing, China, [4]CAS Center for Excellence in Tibetan Plateau Earth Sciences, Beijing, China, [5]School of Earth Sciences, China University of Geosciences, Wuhan, China, [6]School of Geography, Liaoning Normal University, Dalian, China, [7]School of Geographic Sciences, Xinyang Normal University, Xinyang, China

OPEN ACCESS

Edited by:
Shiyong Yu,
Jiangsu Normal University, China

Reviewed by:
Weiguo Liu,
Chinese Academy of Sciences, China
Nadia Solovieva,
University College London, United Kingdom

***Correspondence:**
Juzhi Hou
houjz@itpcas.ac.cn

Specialty section:
This article was submitted to Quaternary Science, Geomorphology and Paleoenvironment, a section of the journal Frontiers in Earth Science

Received: *19 June 2020*
Accepted: *17 August 2020*
Published: *02 September 2020*

Citation:
He Y, Hou J, Wang M, Li X, Liang J, Xie S and Jin Y (2020) Temperature Variation on the Central Tibetan Plateau Revealed by Glycerol Dialkyl Glycerol Tetraethers From the Sediment Record of Lake Linggo Co Since the Last Deglaciation. Front. Earth Sci. 8:574206. doi: 10.3389/feart.2020.574206

The Tibetan Plateau (TP) has numerous glaciers that provide water for more than one-third of the world's population. Reconstructing past temperature change on the TP provides a valuable context for assessing the current and possible future status of glaciers. However, the quantitative paleotemperature records since the last deglaciation on the TP are sparse. Moreover, existing records have revealed a conflicting Holocene temperature variation patterns on the northeastern and western TP. Quantitative temperature records on the central TP would be essential for a better understanding of the spatiotemporal complexity of temperature variation. In this study, we report the temperature record from the sedimentary record of lake Linggo Co on the central TP since the last deglaciation using branched glycerol dialkyl glycerol tetraethers based proxy. Our results indicate that the paleoclimate during the last deglaciation on the central TP was characterized by large fluctuations in temperature. The mean annual temperature of lake Linggo Co remained low during the early Holocene (11.7–10 ka BP) and gradually increased to 4°C at 8.3 ka, rapidly declining to −2°C on average toward the present day. Solar radiation, continental glacier feedback, as well as atmosphere circulation play a major role in the distribution of sensitive and latent heat, thus affecting the Holocene temperature variability of the TP. Discrepancies in published records on the TP can result from a seasonal bias of the proxies and spatial differences due to topography-boundary effect. Our results suggest that the seasonal bias of proxies, the spatiotemporal difference should be taken into consideration before regional or global synthesis of paleotemperature records.

Keywords: Tibetan Plateau, Linggo Co, the last deglaciation, paleotemperature, glycerol dialkyl glycerol tetraethers

INTRODUCTION

The Tibetan Plateau (TP) is the world's highest and largest plateau, which has numerous glaciers that provide water for more than one-third of the world's population (Qiu, 2008). During the last few decades, glaciers on the TP have experienced rapid and pronounced changes (Yao et al., 2019; Immerzeel et al., 2020), increasing concern about water management and geohazards (Kääb et al., 2018; Veh et al., 2020). The significant changes in glaciers, on one hand, can be attributed to changing precipitation patterns (Yao et al., 2012). For example, in the western TP, glacier advanced due to the climatic influence of the mid-latitude westerlies, whereas glaciers in the southern and eastern TP have retreated because of the decreased influence of monsoonal precipitation (Yao et al., 2012). Additionally, temperature plays a critical role in the stability of glaciers (Bolch et al., 2012; Jacob et al., 2012; Neckel et al., 2014). Meteorological observations and climate modeling results have revealed that temperature variations at higher elevations are more significant than that at lower elevations (Bradley et al., 2006; Liu et al., 2009). Reconstructing past temperature change on the TP provides a valuable context for assessing the current and possible future status of glaciers.

Numerous papers have comprehensively discussed the interplay between Asian summer monsoon (ASM) and westerlies and the associated paleoclimate change on the TP and surrounding regions at various time scales (Dykoski et al., 2005; Herzschuh, 2006; Chen et al., 2008; Wang et al., 2010; An et al., 2012). However, the quantitative paleotemperature records since the last deglaciation on the TP are sparse. Moreover, existing records have revealed a conflicting Holocene temperature variation patterns on the northeastern and western TP (Herzschuh et al., 2006; Lu et al., 2011; Ma et al., 2014; Hou et al., 2016; Li et al., 2017). An early-to-middle Holocene temperature optimum has been widely reported using pollen data (Herzschuh et al., 2006; Lu et al., 2011; Ma et al., 2014). Similarly, two alkenone-based temperature records from Lake Qinghai, on the northeastern TP, reveal a cooling trend from the early to the middle Holocene (Wang Z. et al., 2015; Hou et al., 2016), whereas a warm and wet early Holocene and cool and dry middle Holocene have been reported for Aweng Co on the western TP (Li et al., 2017). Quantitative temperature records on the Central TP would be essential for a better understanding of the spatiotemporal complexity of temperature variation.

Glycerol dialkyl glycerol tetraethers (GDGTs) are membrane lipids that can be synthesized by both archaea [isoprenoid GDGTs (iGDGTs)] and bacteria [branched GDGTs (bGDGTs)] (Schouten et al., 2013). These GDGTs are ubiquitous in marine and terrestrial environments (Schouten et al., 2013). For iGDGTs, TEX_{86} [tetraether index of 86 carbon atoms (Schouten et al., 2002)] has been demonstrated to positively correlate with temperature growth in incubation experiments (Wuchter, 2004; Schouten et al., 2007), oceans (Schouten et al., 2002; Kim et al., 2008; Kim et al., 2010), and in some large lakes (Powers et al., 2004; Blaga et al., 2008; Powers et al., 2010). For the TP, Wang et al. (2012) reported that there was a minor influence of terrestrial input on TEX_{86} in the deepest parts of lake Qinghai. Günther et al. (2014) investigated GDGTs in nine lake areas on the TP, suggesting that TEX_{86} still seems relatively suitable for lake water reconstruction.

As regards bGDGTs, Weijers et al. (2007b) found that the cyclization ratio of bGDGTs (CBT) vary with soil pH, whereas the degree of methylation of bGDGTs (MBT) is significantly correlated with soil pH and mean annual air temperature (MAT) based on a survey of global soils. Therefore, the MBT/CBT and its modified version (e.g. MBT′/CBT) proxies have the potential to reconstruct paleotemperature variation (Weijers et al., 2007b; Peterse et al., 2012). With the improvement of analytical methods, a series of 6-methyl bGDGTs, which are co-eluted with 5-methyl bGDGTs, were identified (De Jonge et al., 2013). The newly defined MBT_{5ME}' proxy is no longer related to soil pH, and significantly improve the correlation with MAT (De Jonge et al., 2014). To date, MBT/CBT, MBT′/CBT and MBT_{5ME}' proxies have been widely used for continental paleotemperature reconstruction (Weijers et al., 2007a; Schouten et al., 2008; Bendle et al., 2010; Zhao et al., 2017; Lu et al., 2019). The lacustrine bGDGTs were initially thought to be derived from soil input, allowing the application of bGDGTs based proxies in lake sediment (Hopmans et al., 2004; Blaga et al., 2008). Later, more and more studies revealed the *in situ* production of bGDGTs in water column or sediment (Sinninghe Damsté et al., 2009; Tierney and Russell, 2009; Pearson et al., 2011). Nevertheless, the distribution of bGDGTs in lake surface sediment has still been found to be strongly correlated with temperature (Sun et al., 2011; Günther et al., 2014; Foster et al., 2016; Dang et al., 2018; Russel et al., 2018). Subsequently, lake specific transfer functions at regional scale have been widely used in reconstructing past temperature change (Günther et al., 2015; Li et al., 2017; Feng et al., 2019).

In this study, we present a GDGTs-inferred, paleotemperature record since the last deglaciation from lake Linggo Co on the central TP. Combining with previous published δD records from the same sediment core (He et al., 2017), we are aiming to reconstruct the paleoclimate variation of the central TP, to discuss the factors that contribute to the spatiotemporal difference of temperature variation on the TP, which is important for regional or global paleotemperature synthesis.

MATERIALS AND METHODS

Field Sampling and Age Determination

Lake Linggo Co (88°35′E, 33°51′N) is a closed basin lake in the western slope of the Puruogangri Glacier on the central TP (**Figure 1A**; Lei et al., 2012). The lake is mainly fed by glacier meltwater and precipitation, with a surface area of ~100 km^2 (Lei et al., 2012).

The *in situ* observation at the Shuanghu meteorological station (~100 km southwest of lake Linggo Co) from October 2011 to September 2013 demonstrates that the mean annual temperature measured is −3.9°C, with a July average temperature of about 7°C, down to average temperature of approximately −15°C in January (Ma et al., 2015). The total annual precipitation is 282.7 mm, with 70–80% of rainfall occurring in summer (Li et al., 2006). The lake is ice covered from December to March (Pan et al., 2012).

A 987-cm-long sediment core (LGC 2011-3) was collected from the lake center at a water depth of 60 m using a UVITEC piston corer in 2011 (**Figure 1B**; He et al., 2017). The chronology of LGC 2011-3 was constructed based on ^{210}Pb measurement taken from the upper

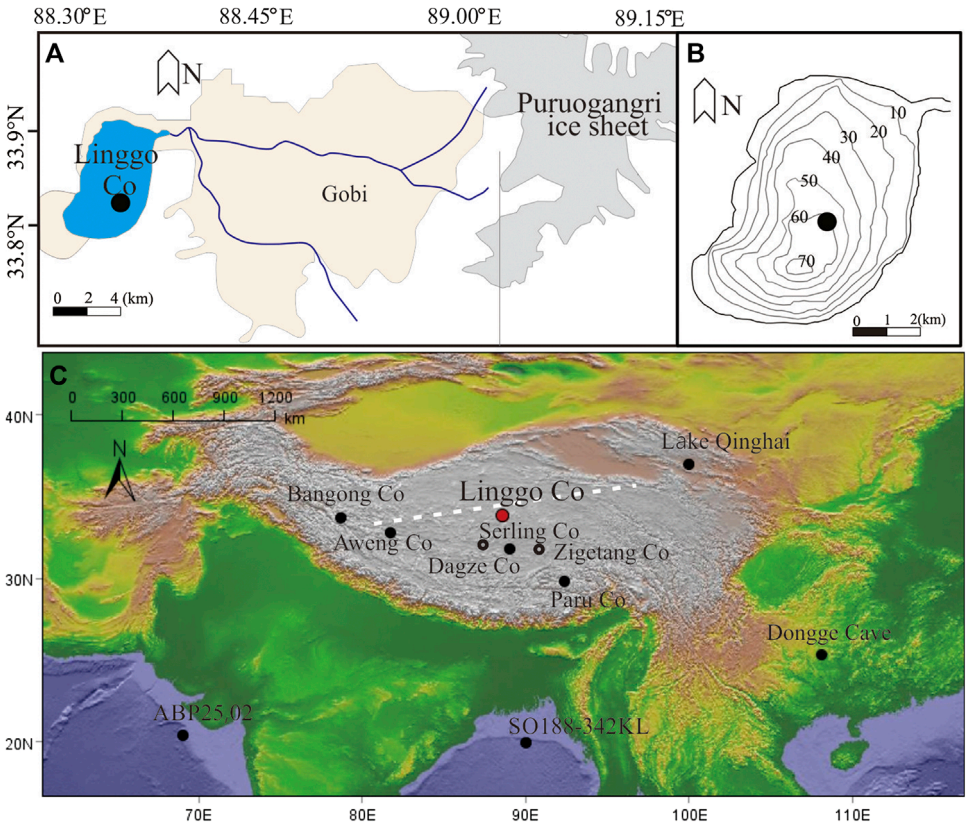

FIGURE 1 | Location of lake Linggo Co and other records mentioned in the text. **(A)** Lake Linggo Co and Puruogangri ice sheet. **(B)** Bathymetry map of lake Linggo Co. Numbers stand for water depth, in meters. Solid circle shows the coring site. **(C)** Other records discussed in text. The dashed line indicates the northern most boundary of Asian summer monsoon (redrawn from Tian et al., 2007).

15 cm of the sediment core, AMS ^{14}C measurements of 27 total organic carbon and two plant macrofossils samples, as well as optically stimulated luminescence (OSL) dating (He et al., 2017). The age-depth model of LGC 2011-3 has been discussed by Hou et al. (2017).

Briefly, the average accumulative rate was 0.092 cm/a in the top 15 cm of the core based on ^{210}Pb results (Hou et al., 2017). The reservoir ages were calculated based on ^{14}C age differences between the plant macrofossils and linearly fitted ages of bulk sediment samples from 350 to 950 cm (Hou et al., 2017). At a depth of 614 cm the difference was 1,788 years, and at a depth of 763 cm, the difference was 1,435 years (Hou et al., 2017). Therefore, we used the mean value for the two reservoir ages (1,611 years) as an average reservoir age throughout the sediment core (Hou et al., 2017). This study only focuses on the record below 350 cm (~4 ka BP) which have convincing chronologic controls from both ^{14}C and OSL dating results (Hou et al., 2017). The significant correlation of the lake Linggo Co records with region records and Indian monsoon records support the chronology at lake Linggo Co (He et al., 2017; Hou et al., 2017).

Glycerol Dialkyl Glycerol Tetraethers Analysis

GDGTs in lake sediments were extracted, as described in Wang et al. (2016). Samples weighing about 5 g were ultrasonically extracted with dichloromethane (DCM) and methanol (9:1, 3 min × 15 min). The total extract was chromatographed using an activated Al_2O_3 column (for 2 h at 150°C). Apolar fraction was eluted by hexane:dichloromethane (9:1), and the polar fraction containing the GDGTs was eluted by DCM:methanol (1:1, three column volumes). After evaporation of the solvents, the polar fraction was redissolved in the mixture of hexane:isopropanol (99:1). The dissolved polar fraction was finally filtered through a 0.45 μm polytetrafluoroethylene (PTFE) filter attached to a 1 ml syringe.

GDGT composition was analyzed on high performance liquid chromatography/atmospheric pressure chemical ionization-mass spectrometry (HPLC-APCI-MS, Agilent 1260 HPLC, MS: 6100) at the Institute of Tibetan Plateau Research, Chinese Academy of Sciences (ITPCAS). Separation was achieved using the Grace Prevail Cyano (150 mm × 2.1 mm, 3 μm), maintained at 40°C. The injection volume was 20 μl. GDGTs were eluted with 90% *A* and 10% *D* for 5 min, followed by a linear gradient to 18% *D* in 45 min, where *A* is hexane (Hex) and *D* is Hex:isopropanol (IPA) = 9:1. Detection was conducted using APCI-MS. The experimental conditions were as follows: the nebulizer pressure was 60 psi, the vaporizer temperature 400°C, the flow rate of drying gas 6 L/min and the temperature 200°C, the capillary voltage (VCap) 3,600 V, and the corona 5.5 μA. GDGTs were detected using selected ion monitoring.

After the separation of 5- and 6-methyl bGDGTs (De Jonge et al., 2014), fifteen samples were reanalyzed based on the updated method, as described by Feng et al. (2019). The polar fractions

were redissolved in 300 μl *n*-hexane:ethyl acetate (EtOA) (84:16, v/v), and the injection volume was 20 μl. Separation of 5- and 6-methyl brGDGTs isomers was done using three Hypersil Gold Silica LC columns in sequence (each 100 mm × 2.1 mm, 1.9 μm; Thermo Fisher Scientific, United States), maintained at 40°C. GDGTs were eluted isocratically with 84% *A* and 16% *B* for the first 5 min, where *A* = *n*-hexane and *B* = ethyl acetate, followed by a linear gradient change to 82% *A* and 18% *B* from 5 to 65 min and then to 100% *B* for 21 min, followed by 100% *B* for 4 min to wash the column and then back to 84% *A* and 16% B to equilibrate the column. The flow rate was 0.2 ml/min throughout the test. Detection was conducted using positive ion APCI of the eluent. The APCI-MS conditions were as follows: the nebulizer pressure was 60 psi, the vaporizer temperature 400°C, the drying gas flow rate 6 L/min and temperature 200°C, the VCap 3,500 V, and the corona 5 μA. Quantification of GDGT compounds was achieved by integrating the areas of the $[M + H]^+$ peaks and comparing these with an external standard curve composed of known GDGTs.

Glycerol Dialkyl Glycerol Tetraethers-Based Proxy Calculation

The MBT and CBT indices were calculated as follows:

$$\mathrm{MBT} = \frac{\mathrm{Ia} + \mathrm{Ib} + \mathrm{Ic}}{\mathrm{Ia} + \mathrm{Ib} + \mathrm{Ic} + \mathrm{IIa} + \mathrm{IIb} + \mathrm{IIc} + \mathrm{IIIa} + \mathrm{IIIb} + \mathrm{IIIc}} \quad (1)$$

after Weijers et al. (2007b).

$$\mathrm{MBT}' = \frac{\mathrm{Ia} + \mathrm{Ib} + \mathrm{Ic}}{\mathrm{Ia} + \mathrm{Ib} + \mathrm{Ic} + \mathrm{IIa} + \mathrm{IIb} + \mathrm{IIc} + \mathrm{IIIa}} \quad (2)$$

after Peterse et al. (2012).

$$\mathrm{CBT} = -\log\frac{\mathrm{Ib} + \mathrm{IIb}}{\mathrm{Ia} + \mathrm{IIa}} \quad (3)$$

after Weijers et al. (2007b).

After the separation of 5- and 6-methyl bGDGTs, $\mathrm{MBT}_{5\mathrm{ME}}'$ was calculated as

$$\mathrm{MBT}'_{5\mathrm{ME}} = \frac{\mathrm{Ia} + \mathrm{Ib} + \mathrm{Ic}}{\mathrm{Ia} + \mathrm{Ib} + \mathrm{Ic} + \mathrm{IIa} + \mathrm{IIb} + \mathrm{IIc} + \mathrm{IIIa}}$$

$$\mathrm{MBT}'_{6\mathrm{ME}} = \frac{\mathrm{Ia} + \mathrm{Ib} + \mathrm{Ic}}{\mathrm{Ia} + \mathrm{Ib} + \mathrm{Ic} + \mathrm{IIa}' + \mathrm{IIb}' + \mathrm{IIc}' + \mathrm{IIIa}'}$$

after De Jonge et al. (2014).

The Branched and Isoprenoid Tetraether (BIT) index was calculated according to

$$\mathrm{BIT} = \frac{\mathrm{Ia} + \mathrm{IIa} + \mathrm{IIIa}}{\mathrm{Ia} + \mathrm{IIa} + \mathrm{IIIa} + \mathrm{Cren}}$$

after Hopmans et al. (2004).

$$\%\mathrm{Tetra} = \sum \text{tetramethylated bGDGTs} = [\mathrm{Ia}] + [\mathrm{Ib}] + [\mathrm{Ic}]$$
$$\%\mathrm{Penta} = \sum \text{pentamethylated bGDGTs} = [\mathrm{IIa}] + [\mathrm{IIb}] + [\mathrm{IIc}]$$
$$\%\mathrm{Hexa} = \sum \text{hexamethylated bGDGTs} = [\mathrm{IIIa}] + [\mathrm{IIIb}] + [\mathrm{IIIc}]$$

after Sinninghe Damsté (2016).

TEX_{86} was calculated using the following the equation:

$$\mathrm{TEX}_{86} = \frac{\mathrm{GDGT} - 2 + \mathrm{GDGT} - 3 + \mathrm{Cren}'}{\mathrm{GDGT} - 1 + \mathrm{GDGT} - 2 + \mathrm{GDGT} - 3 + \mathrm{Cren}'}$$

after Schouten et al. (2002).

The methane index (MI) was calculated using the following:

$$\mathrm{MI} = \frac{\mathrm{GDGT} - 1 + \mathrm{GDGT} - 2 + \mathrm{GDGT} - 3}{\mathrm{GDGT} - 1 + \mathrm{GDGT} - 2 + \mathrm{GDGT} - 3 + \mathrm{Cren} + \mathrm{Cren}'}$$

after Zhang et al. (2011).

The %Cren′ values were calculated as follows:

$$\%\mathrm{Cren}' = \frac{\mathrm{Cren}'}{\mathrm{GDGT} - 0 + \mathrm{GDGT} - 1 + \mathrm{GDGT} - 2 + \mathrm{GDGT} - 3 + \mathrm{Cren} + \mathrm{Cren}'}$$

after Wang H. et al. (2015).

RESULTS

Relative Concentrations of Glycerol Dialkyl Glycerol Tetraethers

Five iGDGTs and nine bGDGTs were detected in all the sediment samples (**Figure 2**). The concentrations of Crenarchaeol′ were below the detection limit for most samples. Hexamethylated, pentamethylated, and tetramethylated brGDGTs constitute 33, 38, and 29% of the major brGDGTs on average (**Figure 3**). A remarkable feature of the GDGTs records is the large differences in the distributions between the last deglaciation and the Holocene.

During the last deglaciation, the bGDGTs and iGDGTs consist of 72.8 and 27.2% of the total GDGTs respectively (**Figure 2**). The domination of bGDGTs leads to high BIT values (from 0.45 to 0.95, **Figure 4A**). Large fluctuations are also observed in MBT′ (as well as in $\mathrm{MBT}_{5\mathrm{ME}}'$, and $\mathrm{MBT}_{6\mathrm{ME}}'$), CBT, and TEX_{86} [**Figures 4B–D**]. During the Holocene, the domination of Crenarchaeol (48.5% of total GDGTs on average, **Figure 2**) leads to low BIT values (0.04–0.20), except for an interval between 7.6 and 8.9 ka BP (0.07–0.61, **Figure 4A**). All the indexes (MBT′, CBT and TEX_{86}) sharply decrease at ~7.6 ka BP (**Figures 4B–D**).

Glycerol Dialkyl Glycerol Tetraethers-Induced Temperature Variation

Most of the MBT′/CBT calibration functions for the TP [e.g., Günther et al. (2014); Wang et al. (2016)] revealed a similar trend in the sedimentary record from lake Linggo Co. Therefore, we use the equation:

$$\mathrm{MAT} = -3.84 + 9.84 \times \mathrm{CBT} + 5.92 \times \mathrm{MBT}' \quad (4)$$

after Günther et al. (2014), which incorporates a similar composition of bGDGTs to that of lake Linggo Co (**Figure 3**) and produces temperature values close to those of the instrumental data.

All the equations based on $\mathrm{MBT}_{6\mathrm{ME}}'$ (Dang, 2017) and $\mathrm{MBT}_{5\mathrm{ME}}'$ [e.g., the equation in Russell et al. (2018) based on

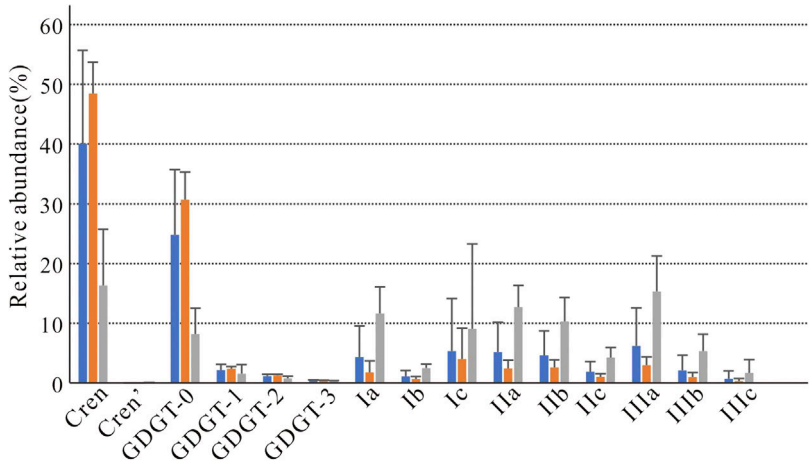

FIGURE 2 | Bar plot showing the fractional abundance (expressed as a percentage of the total) of glycerol dialkyl glycerol tetraethers (GDGTs) in LGC 2011-3 (without the separation of 5- and 6-methyl bGDGTs). Blue bars represent the samples of all the samples, orange bars stand for the samples during the Holocene, gray bars stand for the samples during the last deglaciation. The raw data can be found in **Supplementary Material**.

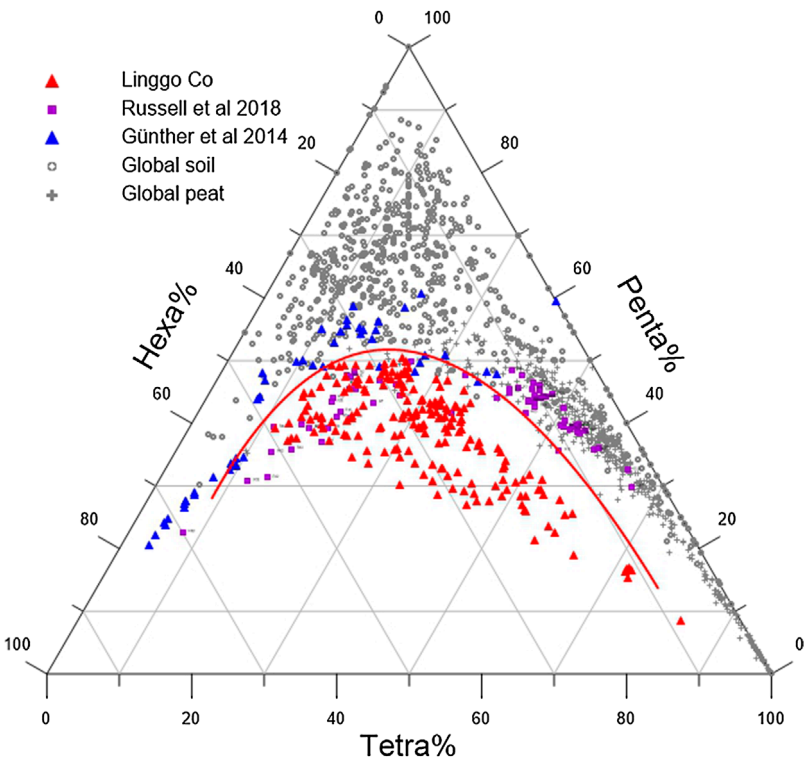

FIGURE 3 | Ternary diagram showing the fractional abundances of tetra-, penta-, and hexamethylated bGDGTs of global soil (Crampton-Flood et al., 2020), global peat (Naafs et al., 2017), lake sediments of the Tibetan Plateau (Günther et al., 2014), East Africa (Russell et al., 2018), and LGC 2011-3 samples (this study).

lake sediments in East Africa and the equation in De Jonge et al. (2014) based on global soil] have similar trends in lake Linggo Co. Considering that the composition of GDGTs in Russell et al. (2018) is close to that of lake Linggo Co (**Figure 3**), we used the equation after Russell et al. (2018):

$$MAT = -1.21 + 32.42 \times MBT'_{5ME}$$

Due to the lack of a TEX_{86}-inferred temperature equation for the TP, the global lake calibration equation was used after Powers et al. (2010):

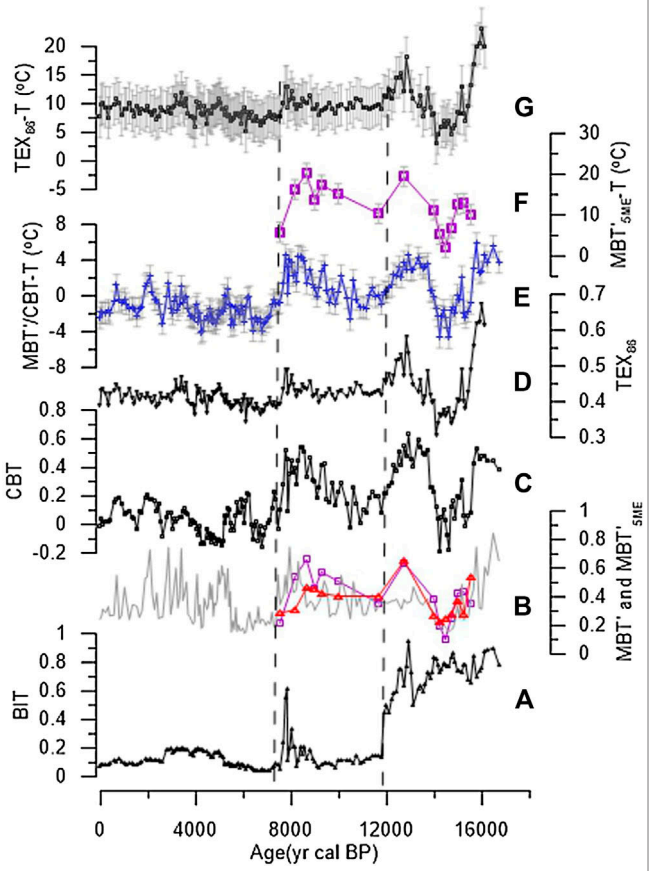

FIGURE 4 | Variation in glycerol dialkyl glycerol tetraethers (GDGTs)-based proxies of lake Linggo Co record. **(A)** Branched and Isoprenoid Tetraether (BIT) index, **(B)** modified methylation index of branched tetraethers (MBT′, black) and its modified index (MBT_{5ME}′, purple; MBT_{6ME}′, red), **(C)** cyclization ratio of bGDGTs (CBT), **(D)** tetraether index of 86 carbon atoms (TEX_{86}), **(E)** MBT′/CBT-induced temperature according to Günther et al. (2014), **(F)** MBT_{5ME}′-induced temperature according to Russell et al. (2018), and **(G)** TEX_{86}-inferred temperature after Powers et al. (2010).

$$LST = 55.231 \times TEX_{86} - 13.955$$

The MBT′/CBT-induced temperature range is from −4.7 to 5.9°C during the last deglaciation, with the coldest period at ~14 ka BP. The average temperature of the early Holocene is ~3°C, which is ~1.2°C higher than that of the middle-to-late Holocene (**Figure 4E**). The MBT_{5ME}′- and TEX_{86}-induced temperature exhibits similar variation and larger fluctuations compared with that of MBT′/CBT (**Figures 4F,G**).

DISCUSSION

Provenance of Glycerol Dialkyl Glycerol Tetraethers

Since bGDGTs are membrane lipids produced by bacteria, sources of bGDGTs in lake sediments can be diverse, comprising, for example, soils (Weijers et al., 2007b), peats (Weijers et al., 2006; Naafs et al., 2017), and aquatic environments (Zhu et al., 2011; Buckles et al., 2014; Sinninghe Damsté, 2016). Therefore, the provenance of bGDGTs should be assessed before using bGDGTs in paleotemperature reconstruction (Yang et al., 2013; Zell et al., 2013; De Jonge et al., 2015; Warden et al., 2016). It has been reported that the ternary diagram of tetra-, penta-, and hexa-methylated bGDGTs can separate bGDGTs from soils by input from land (e.g., by riverine transport) or by aquatic (*in situ*) production (Sinninghe Damsté, 2016). For lake Linggo Co, all samples are distinguished with global soil (Crampton-Flood et al., 2020) or peat samples (Naafs et al., 2017) (**Figure 3**), implying that the bGDGTs are produced *in situ* in the water column. Previous studies have found bGDGTs in soil, suspend paniculated matter in the river and settling particulate matter in traps all year round (Weijers et al., 2011; Loomis et al., 2014; Cao M. et al., 2018). Thus, the reconstructed MAT represents the annual mean temperature of lake water.

As regards iGDGTs, it should address that iGDGTs are derived predominantly from thaumarchaeota living in the water column before using as a lacustrine paleotemperature proxy (Sinninghe Damsté et al., 2012). Using the approach of Sinninghe Damsté et al. (2012) and Wang H. et al. (2015), we critically excluded two samples at 775 and 845 cm that had GDGT-0/Cren > 2, MI > 0.24, or %Cren′ isomer > 2 for the LGC-2011 record.

The MBT′/CBT-inferred temperature of the surface sediment is −2.5°C, with a root mean square error of prediction of 1.2°C in the transfer function (Günther et al., 2014). The reconstructed temperature fits well with the instrumental mean annual temperature of −3.7°C (Ma et al., 2015). An annual lake water temperature below zero has also been observed at Dagze Co on the central TP (Wang et al., 2014). The MBT_{5ME}′- and TEX_{86}-induced temperature at lake Linggo Co is clearly overestimated (**Figures 4F,G**); this may be due to the application of the global and east Africa lake calibration functions, rather than a regional function suitable for the TP which has not yet been proposed. Thus, the MBT_{5ME}′- and TEX_{86}-referred temperatures should be considered tendencies rather than absolute values (Günther et al., 2015). Considering that the MBT′/CBT record has the highest resolution, our study was mainly based on the MBT′/CBT record.

Climate Change on the Central Tibetan Plateau Since the Last Deglaciation

It is widely reported that sedimentary leaf waxes (e.g., *n*-alkanes, *n*-fatty acids) record hydrogen isotopes in precipitation (Sachse et al., 2004, 2006; Hou et al., 2008; Sachse et al., 2012). Meteorological observations on the TP have revealed that precipitation in the monsoon domain is more depleted in isotope composition than in the westerly jet domain (Yao et al., 2013). A strong ASM would deliver more monsoonal precipitation which is depleted in $\delta^{18}O$ (as well as δD). In contrast, a weak ASM would give rise to a greater moisture delivered by the local recycle or westerly jet which is less depleted in $\delta^{18}O$ (δD) (Tian et al., 2007; Yao et al., 2013). Therefore, the *n*-fatty acid δD records of lake Linggo Co represent the amount of monsoonal precipitation (He et al., 2017; Hou et al., 2017).

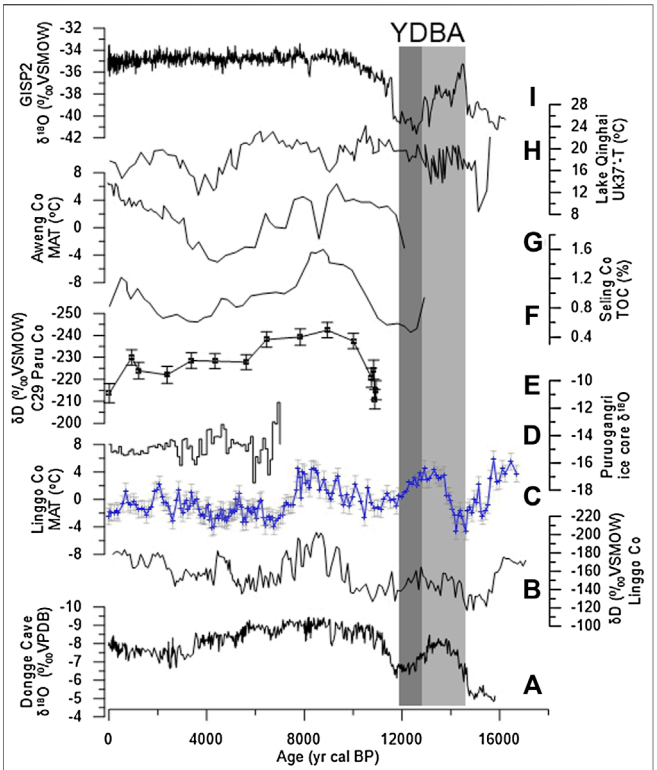

FIGURE 5 | Comparison between lake Linggo Co temperature records and other records for the Tibetan Plateau. **(A)** $\delta^{18}O$ record in Dongge Cave (Dykoski et al., 2005), **(B)** weighted hydrogen isotope value of long chain n-fatty acids of lake Linggo Co (He et al., 2017), **(C)** MBT′/CBT-induced temperature records of lake Linggo Co (this study), **(D)** $\delta^{18}O$ record of Puruogangri ice core (Thompson et al., 2006), **(E)** δD of C29 *n*-alkanes in Paru Co (Bird et al., 2014), **(F)** total organic matter concentration of Serling Co (Zhu et al., 2019), **(G)** MBT′/CBT-induced temperature record in Aweng Co (Li et al., 2017), **(H)** alkenone-based temperature records for Lake Qinghai (Hou et al., 2016), and **(I)** $\delta^{18}O$ record of GISP2 (Stuiver and Grootes, 2000). Gray bars represent widely reported periods like the Younger–Dryas and BA warm period.

Combining the MBT′/CBT-induced temperature with δD records of lake Linggo Co, we can reconstruct the paleoclimate fluctuations of the central TP since the last deglaciation.

The Last Deglaciation

The last deglaciation was characterized by large fluctuations in temperature (from −4.7 to 5.9°C) and the domination of local recycled moisture. The coldest periods occurred at ~14 ka BP. The temperature increased by ~6°C from 13.5 to 12.5 ka BP, likely corresponding to the Bølling–Allerød (BA) warming period (Grootes et al., 1993; Shakun et al., 2012). Following the BA warming period, temperature and δD returned to those values of cold and dry conditions, coincident in timing with a Younger Dryas (YD) event. All these events (BA and YD) in lake Linggo Co appear to be nearly synchronous with other records in Monsoonal Asia [e.g., the $\delta^{18}O$ record in Dongge cave (Dykoski et al., 2005), **Figure 5A**] and high latitude records in northern hemisphere [e.g., the $\delta^{18}O$ record of GISP2 (Stuiver and Grootes, 2000), **Figure 5I**]. For the TP, the UK'^{37}-inferred temperature in Lake Qinghai (Hou et al., 2016; **Figure 5H**) also have the same trend.

Global climate modeling has demonstrated that the growth of ice sheet and the decrease of North Atlantic sea surface temperature during the Last Glacial Maximum give rise to an increase in the latitudinal temperature gradient and southward migration of the westerlies (COHMAP members, 1988; Kutzbach et al., 1993; Jiang et al., 2015). Therefore, the westerly jet may have dominated during the last deglaciation, transferring the climatic signal from a high northern latitude to the TP. On the other hand, due to the long distance from oceanic moisture source, the ASM can hardly reach the central TP (An et al., 1991). The strong westerlies and weak ASM contribute to the cold and dry climate on the TP.

The Holocene

During the Holocene, the MAT from lake Linggo Co remains low prior to 10 ka BP and gradually increases to 4°C at 8.3 ka BP (**Figure 6A**), which have around 2,000 years delay relative to the peak of summer insolation (**Figure 6G**). The peak annual temperature at ~8.3 ka BP is followed by a rapid decline in temperature to −2°C, on average, to the present day. This trend is closely associated with monsoonal precipitation variation inferred by the δD record from the same core (**Figure 6B**). The significant correlation between monsoonal precipitation and temperature implies the importance of latent heat to the energy budget on

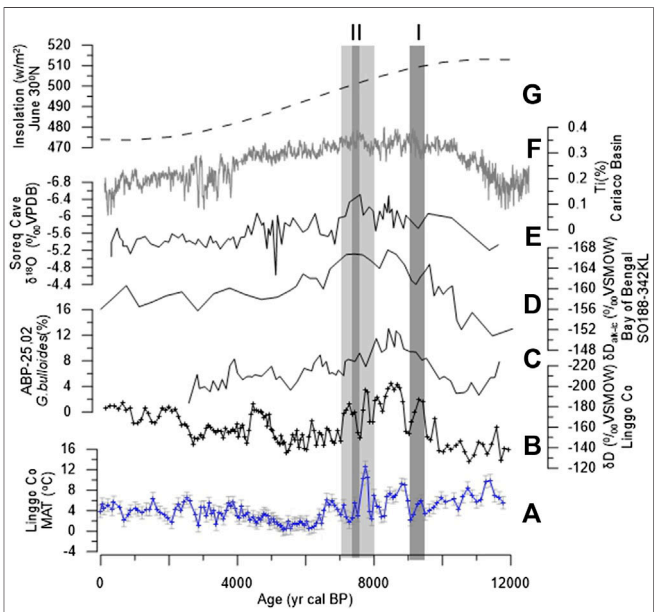

FIGURE 6 | Comparison between lake Linggo Co Holocene temperature variation records and other records in monsoonal Asian. **(A)** MBT′/CBT-induced temperature records of lake Linggo Co (this study), **(B)** weighted hydrogen isotope value of long chain n-fatty acids of lake Linggo Co (He et al., 2017), **(C)** percentage of *Globigerina bulloides* from Hole ABP-25, 02, from the northeastern Arabian Sea (Gupta et al., 2011), **(D)** δD record from the Bay of Bengal (SO188–342KL, Contreras-Rosales et al., 2014), **(E)** $\delta^{18}O$ record in Soreq Cave (Bar-Matthews and Ayalon, 1997), **(F)** Ti from Cariaco basin (Haug et al., 2001), and **(G)** June insolation at 30 N (Berger and Loutre, 1991). Gray bars represent the disappearance of the Fennoscandian (I) and Laurentide (II) ice sheets according to Carlson (2008).

the TP, which is evidenced by modern observation (Shi and Liang, 2014; Li et al., 2015). During the pre-monsoon period, the sensible heat flux is the major energy source of the TP (Shi and Liang, 2014; Li et al., 2015). Whereas in the monsoon season, the water vapor, in form of monsoonal precipitation, transfer the energy from low latitude to the TP (An et al., 2015), the released latent heat flux is even greater than the sensible heat flux (Li et al., 2015).

At the beginning of the early Holocene (~11.5 ka BP), summer insolation in the Northern Hemisphere reaches a maximum (Berger and Loutre, 1991) (**Figure 6G**), resulting in an increase in sensitive heat in summer. Many records for the TP [e.g., Aweng Co in western TP (Li et al., 2017) and Lake Qinghai in northeastern TP (Hou et al., 2016), **Figures 5G,H**] show an increase in temperature in the early Holocene. The summer temperature increase is also evidenced in the high lake level of lake Linggo Co in the early Holocene based on OSL dating results from the paleo-shore sand samples (Pan et al., 2012). As monsoonal precipitation is limited during this period (He et al., 2017), the increased lake water level most likely originated from the accelerated melting of the Puruogangri ice sheet in response to increasing summer temperature. Notably, the winter insolation was weak during this period. The cooling effect of the Puruogangri ice sheet and the weak winter insolation may have compensated for the strong summer insolation; meanwhile, limited latent heat from monsoonal precipitation caused a rise in the relatively low temperature during 11.7–10 ka BP in lake Linggo Co.

As the continental ice sheets and glaciers continuously retreated (Kurt et al., 2014), the Interhemispheric Thermal Gradients gradually increased, driving the mean latitudinal position of the Intertropical convergence zone (ITCZ) northward (Kutzbach et al., 1993; Renssen et al., 2009). The monsoonal precipitation arrived at lake Linggo Co until ~10 ka BP, released more latent heat and raised the temperature. At ~7.8 ka BP, the disappearance of the Laurentide ice sheet (Carlson, 2008) led to the interhemispheric thermal gradients reaching a maximum (**Figure 6**). Consequently, the ITCZ expanded to the furthest northward position (Schneider et al., 2014). The latent heat from monsoonal precipitation also reached a maximum, leading to a thermal maximum on the central TP (**Figures 6B,C**).

After ~7.8 ka BP, the summer insolation began to decrease (Berger and Loutre, 1991). Latent heat associated with monsoonal precipitation gradually decreased, resulting in southward migration of the ITCZ. Moreover, the weak ISM may give rise to a short summer season (Chiang et al., 2015), shortening the period for heat exchange between lake water and atmosphere. Therefore, the bGDGTs-derived lake water temperature is closer to that in cold season. The westerlies may also have become strengthened during this period. For example, the lake level at Accesa in the Mediterranean increased during the middle Holocene, in response to a northward migration of westerlies as latitudinal temperature gradient decreased (Magny et al., 2013). The strong westerlies suppressed moisture supply (as well as latent heat supply) to the TP (Bothe et al., 2010), giving rise to a decrease in MAT in lake Linggo Co during the middle Holocene. The $\delta^{18}O$ record of the Puruogangri ice core (**Figure 5D**), which represents temperature, also shows cooling after the middle Holocene (Thompson et al., 2006).

The late arrival of ASM at ~10 ka BP and its early retreat during the middle Holocene is also evidenced in other records of the TP interior. For example, the δD record from Paru Co (**Figure 5E**) indicates that maximal monsoonal precipitation occurs between 10.1 and 5.2 ka BP (Bird et al., 2014). The TOC record in Serling Co (**Figure 5F**) also suggests a thermal maximum between 10.5 and 7.6 ka BP (Zhu et al., 2019). For the TP, the weakening of monsoon intensity after the middle Holocene is preserved in many records in east and south Asia: for example, the percentage of *Globigerina bulloides* from Hole ABP-25, 02, in the northeastern Arabian Sea (**Figure 6C**; Gupta et al., 2011), the δD record from SO188–342KL in the Bay of Bengal (**Figure 6D**; Contreras-Rosales et al., 2014), the $\delta^{18}O$ record in Soreq cave (**Figure 6E**; Bar-Matthews and Ayalon, 1997), and the concentration of Ti in the Cariaco basin (**Figure 6F**; Haug et al., 2001).

The Spatiotemporal Patterns of Holocene Temperature Variation of the Tibetan Plateau

Holocene temperature variations have attracted much attention in recent years (Marcott et al., 2013; Liu Z. et al., 2014; Marsicek et al., 2018; Hou et al., 2019; Lin et al., 2019; Park et al., 2019; Kaufman et al., 2020). Marcott et al. (2013) compiled 73 quantitative temperature records worldwide and retrieved a pattern of early Holocene (10–5 ka BP) warmth followed by 0.7°C of cooling through the middle to the late Holocene (<5 ka BP). However, based on three different transient climate models forced by orbital-driven insolation variations, greenhouse gases, and continental ice sheets and the associated meltwater fluxes, Liu Z. et al. (2014) reported a gradual Holocene warming with an absence of late Holocene cooling. Liu Z. et al. (2014) further suggested that the model-data inconsistency could result from the seasonality of the current temperature proxies and the inadequacy of current climate models.

Apparently, the Holocene temperature variation of lake Linggo Co differs from previously published pollen assemblage (Herzschuh et al., 2006; Lu et al., 2011; Ma et al., 2014) and alkenone-based temperature records for the TP. For example, Herzschuh et al. (2006) revealed a general cooling trend throughout the Holocene based on pollen data from Zigetang Co, on the central TP. Two recent alkenone-based temperature records also suggest a cooling trend from the early to the middle Holocene for Lake Qinghai, northeastern TP (Wang Z. et al., 2015; Hou et al., 2016). Many factors may contribute to this discrepancy.

Seasonal bias of the proxy is part of the reason of this discrepancy. For alkenones, the temperature of the growing season of haptophytes can influence the ratios of unsaturated compounds; thus, UK^{37} reflects warm season temperatures at high altitudes and cool season temperatures at low latitudes (Schneider et al., 2010). Therefore, the alkenone-based temperature records from lake Qinghai were mainly interpreted as summer temperature (Hou et al., 2016). For pollen assemblages, it has the potential to reconstruct both seasonal and annual mean temperature (e.g., Davis et al., 2003). The quality of reconstructed temperature (as well as precipitation) strongly depends on the choice of pollen-climate calibration sets (Cao X. et al., 2018).

Considering the harsh environment in cold season on the TP, the pollen record on the TP may have a more sensitive response to summer temperature, which is also evidenced in the study from southeast Idaho, United States (Lundeen and Brunelle, 2016). With respect to bGDGTs, the seasonal bias of the proxy is still controversial (Weijers et al., 2011; Loomis et al., 2014; Cao M. et al., 2018). Some authors suggest there is no apparent seasonal bias due to the following: 1) bGDGTs are produced in soil, in riverine suspended particulate matter, and in particulate matter settled in traps all year round (Weijers et al., 2011; Cao M. et al., 2018); 2) the turnover time of ~20 years for bGDGTs can smooth monthly variation (Weijers et al., 2011). Some authors argue that the flux of bGDGTs in sediments is highest during spring and fall isothermal mixing, potentially biasing paleotemperature reconstruction toward mixing season temperatures (Loomis et al., 2014). Dang et al. (2018) found a seasonal bias toward warm months in the Chinese lakes for cold regions. For lake Linggo Co, as discussed above, most of the bGDGTs are *in situ* produced in the water column or the sediment likely all year round. Therefore, the bGDGTs derived temperature is annual mean temperature of lake water. In any case, the seasonal bias of the proxies associated with their difference in biosynthesis way required caution treatment before regional or global synthesis of paleotemperature records.

The discrepancy between lake Linggo Co and other records on TP may also result from the spatial complexity due to the interplay of westerlies and ASM on the TP. Liu X. J. et al. (2014) proposed that a climate threshold existed for the penetration of Asian monsoon rainfall into the TP. Evidence for this hypothesis can be found in the different responses of the interior and the edge of the TP to paleoclimate change. At the Pleistocene-Holocene boundary, the margin of the TP served as a barrier to a strengthening and landward-encroaching monsoon system. Therefore, a lake on the edge of the TP (such as Lake Qinghai on the northeastern TP and Bangong and Aweng Co on the western TP) possesses evidence of an increase in temperature and monsoonal precipitation, with no apparent lag in the summer insolation maximum. While lake Linggo Co and Paru Co, in the interior of TP, receive the monsoonal precipitation and latent heat till ~10 ka BP. During the middle Holocene, lake Linggo Co, at the northern-most boundary of ASM, captured the signal of ASM weakening (as well as that of the strengthening of westerlies), while the northeastern and western TP were still under the influence of ASM. The spatiotemporal complex of temperature variation in the TP suggests the importance of having widely distributed site-specific paleotemperature data before regional or global synthesis.

CONCLUSIONS

We report a quantitative mean annual temperature record since the last deglaciation, based on bGDGTs in lake Linggo Co from the central TP. Similar trends in bGDGTs- and iGDGTs-reconstructed temperature give confidence in this record. Our results indicate that the paleoclimate during the last deglaciation on the central TP was characterized by large fluctuations in temperature with the domination of local recycled moisture. The mean annual temperature of lake Linggo Co remained low during the early Holocene (11.7–10 ka BP), gradually increase to 4°C at 8.3 ka BP, and then rapidly decreased to −2°C toward the present. Solar radiation, continental glacier feedback, as well as atmosphere circulation play a major role in the distribution of sensitive and latent heat, thus affecting Holocene temperature variability on the TP. The discrepancies between lake Linggo Co and previous published Holocene temperature records can result from a seasonal bias of the proxy, and spatial complexity on the TP, resulting in a boundary effect. Our results suggest the seasonal bias of the proxy, spatiotemporal differences of temperature variation should be taken into consideration before regional or global synthesis of paleotemperature records.

DATA AVAILABILITY STATEMENT

All datasets presented in this study are included in the article/ **Supplementary Material**.

AUTHOR CONTRIBUTIONS

YH processed the experimental data, performed the analysis, drafted the manuscript; JH supervised the project; MW, XL, JL and SX helped shape the manuscript; YJ modified some of the figures. All authors listed have made a substantial, direct, and intellectual contribution to the work and approved it for publication.

FUNDING

This work was supported by the National Natural Science Foundation of China (Grant Nos. 41903069, 4180020297, 41901105), Natural Science Foundation of Hebei province (Grant Nos. D2020403059, D2018403044), and the Fundamental Research Funds for the Central Universities, China University of Geosciences (Wuhan) (Grant No. CUG170104).

SUPPLEMENTARY MATERIAL

The Supplementary Material for this article can be found online at: https://www.frontiersin.org/articles/10.3389/feart.2020.574206/full#supplementary-material

REFERENCES

An, Z. S., Colman, S. M., Zhou, W. J., Li, X. Q., Brown, E. T., Jull, A. J. T., et al. (2012). Interplay between the Westerlies and Asian monsoon recorded in Lake Qinghai sediments since 32 ka. *Sci. Rep.* 2, 619. doi:10.1038/Srep00619

An, Z. S., Wu, G. X., Li, J. P., Sun, Y. B., Liu, Y. M., Zhou, W. J., et al. (2015). Global monsoon dynamics and climate change. *Annu. Rev. Earth Plant. Sci.* 43, 29–77. doi:10.1146/annurev-earth-060313-054623

An, Z. S., Wu, X. H., Wang, P. X., Wang, S. M., Dong, G. R., Sun, X. J., et al. (1991). Paleomonsoons of China over the last 130,000 years—Paleomonsoon variation. *Sci. China Ser. B* 34, 1016–1024. doi:10.1006/qres.1999.2072

Bar-Matthews, M., Ayalon, A., and Kaufman, A. (1997). Late quaternary paleoclimate in the eastern Mediterranean region from stable isotope analysis of speleothems at Soreq cave, Israel. *Quat. Res.* 47, 155–168. doi:10.1006/qres.1997.1883

Bendle, J. A., Weijers, J. W. H., Maslin, M. A., Damsté, J. S. S., Schouten, S., Hopmans, E. C., et al. (2010). Major changes in glacial and Holocene terrestrial temperatures and sources of organic carbon recorded in the Amazon fan by tetraether lipids. *G-Cubed* 11, 1–70. doi:10.1029/2010gc003308

Berger, A., and Loutre, M. F. (1991). Insolation values for the climate of the last 10 million years. *Quat. Sci. Rev.* 10, 297–317. doi:10.1016/0277-3791(91)90033-q

Bird, B. W., Polisar, P. J., Lei, Y., Thompson, L. G., Yao, T., Finney, B. P., et al. (2014). A Tibetan lake sediment record of Holocene Indian summer monsoon variability. *Earth Planet. Sci. Lett.* 399, 92–102. doi:10.1016/j.epsl.2014.05.017

Blaga, C. I., Reichart, G. J., Heiri, O., and Sinninghe Damsté, J. S. (2008). Tetraether membrane lipid distributions in water-column particulate matter and sediments: a study of 47 European lakes along a north-south transect. *J. Paleolimnol.* 41, 523–540. doi:10.1007/s10933-008-9242-2

Bolch, T., Kulkarni, A., Kääb, A., Huggel, C., Paul, F., Cogley, J. G., Frey, H., et al. (2012). The state and fate of Himalayan glaciers. *Science* 336, 310–314. doi:10.1126/science.1215828

Bothe, O., Fraedrich, K., and Zhu, X. H. (2010). The large-scale circulations and summer drought and wetness on the Tibetan Plateau. *Int. J. Climatol.* 30, 844–855. doi:10.1002/Joc.1946

Bradley, R. S., Vuille, M., Diaz, H. F., and Vergara, W. (2006). Climate change: threats to water supplies in the tropical Andes. *Science* 312, 1755–1756. doi:10.1126/science.1128087

Buckles, L. K., Weijers, J. W. H., Verschuren, D., and Sinninghe Damsté, J. S. (2014). Sources of core and intact branched tetraether membrane lipids in the lacustrine environment: Anatomy of Lake Challa and its catchment, equatorial East Africa. *Geochim. Cosmochim. Acta* 140, 106–126. doi:10.1016/j.gca.2014.04.042

Cao, M., Rueda, G., Rivas-Ruiz, P., Trapote, M. C., Henriksen, M., Vegas-Vilarrúbia, T., et al. (2018). Branched GDGT variability in sediments and soils from catchments with marked temperature seasonality. *Org. Geochem.* 122, 98–114. doi:10.1016/j.orggeochem.2018.05.007

Cao, X., Tian, F., and Ding, W. (2018). Improving the quality of pollen-climate calibration-sets is the primary step for ensuring reliable climate reconstructions. *Sci. Bull.* 63, 1317–1318. doi:10.1016/j.scib.2018.09.007

Carlson, A. E., LeGrande, A. N., Oppo, D. W., Came, R. E., Schmidt, G. A., Anslow, F. S., et al. (2008). Rapid early Holocene deglaciation of the Laurentide ice sheet. *Nat. Geosci.* 1, 620–624. doi:10.1038/ngeo285

Chen, F. H., Yu, Z. C., Yang, M. L., Ito, E., Wang, S. M., Madsen, D. B., et al. (2008). Holocene moisture evolution in arid central Asia and its out-of-phase relationship with Asian monsoon history. *Quat. Sci. Rev.* 27, 351–364. doi:10.1016/j.quascirev.2007.10.017

Chiang, J. C. H., Fung, I. Y., Wu, C.-H., Cai, Y., Edman, J. P., Liu, Y., et al. (2015). Role of seasonal transitions and westerly jets in East Asian paleoclimate. *Quat. Sci. Rev.* 108, 111–129. doi:10.1016/j.quascirev.2014.11.009

COHMAP Members (1988). Climatic changes of the last 18,000 years: observations and model simulations. *Science* 241, 1043–1052. doi:10.1126/science.241.4869.1043

Contreras-Rosales, L. A., Jennerjahn, T., Tharammal, T., Meyer, V., Lückge, A., Paul, A., et al. (2014). Evolution of the Indian Summer Monsoon and terrestrial vegetation in the Bengal region during the past 18 ka. *Quat. Sci. Rev.* 102, 133–148. doi:10.1016/j.quascirev.2014.08.010

Crampton-Flood, E. D., Tierney, J. E., Peterse, F., Kirkels, F. M. S. A., and Sinninghe Damsté, J. S. (2020). BayMBT: a Bayesian calibration model for branched glycerol dialkyl glycerol tetraethers in soils and peats. *Geochim. Cosmochim. Acta* 268, 142–159. doi:10.1016/j.gca.2019.09.043

Damsté, J. S. S., Ossebaar, J., Schouten, S., and Verschuren, D. (2012). Distribution of tetraether lipids in the 25-ka sedimentary record of Lake Challa: extracting reliable TEX_{86} and MBT/CBT palaeotemperature from an equatorial African lake. *Quat. Sci. Rev.* 50, 43–54.

Dang, X. Y. (2017). Impacts of hydrological conditions and temperature on microbial tetraether lipids in soils and lakes: Implications for climatic reconstructions. Doctoral thesis. Wuhan (China): China University of Geosciences.

Dang, X. Y., Ding, W. H., Yang, H., Pancost, R. D., Naafs, B. D. A., Xue, J. T., et al. (2018). Different temperature dependence of the bacterial brGDGT isomers in 35 Chinese lake sediments compared to that in soils. *Org. Geochem.* 119, 72–79. doi:10.1016/j.orggeochem.2018.02.008

Davis, B. A. S., Brewer, S., Stevenson, A. C., and Guiot, J., and Data Contributors (2003). The temperature of Europe during the Holocene reconstructed from pollen data. *Quat. Sci. Rev.* 22, 1701–1716. doi:10.1016/S0277-3791(03)00173-2

De Jonge, C., Hopmans, E. C., Stadnitskaia, A., Rijpstra, W. I. C., Hofland, R., Tegelaar, E., et al. (2013). Identification of novel penta- and hexamethylated branched glycerol dialkyl glycerol tetraethers in peat using HPLC-MS2, GC-MS and GC-SMB-MS. *Org. Geochem.* 54, 78–82. doi:10.1016/j.orggeochem.2012.10.004

De Jonge, C., Hopmans, E. C., Zell, C. I., Kim, J.-H., Schouten, S., and Sinninghe Damsté, J. S. (2014). Occurrence and abundance of 6-methyl branched glycerol dialkyl glycerol tetraethers in soils: implications for palaeoclimate reconstruction. *Geochim. Cosmochim. Acta* 141, 97–112. doi:10.1016/j.gca.2014.06.013

De Jonge, C. D., Stadnitskaia, A., Fedotov, A., and Damsté, J. S. S. (2015). Impact of riverine suspended particulate matter on the branched glycerol dialkyl glycerol tetraether composition of lakes: the outflow of the Selenga River in Lake Baikal (Russia). *Org. Geochem.* 83–84, 241–252.

Dykoski, C. A., Edwards, R. L., Cheng, H., Yuan, D. X., Cai, Y. J., Zhang, M. L., et al. (2005). A high-resolution, absolute-dated Holocene and deglacial Asian monsoon record from Dongge Cave, China. *Earth Planet. Sci. Lett.* 233, 71–86. doi:10.1016/j.epsl.2005.01.036

Feng, X., Zhao, C., D'Andrea, W. J., Liang, J., Zhou, A., and Shen, J. (2019). Temperature fluctuations during the Common Era in subtropical southwestern China inferred from brGDGTs in a remote alpine lake. *Earth Planet. Sci. Lett.* 510, 26–36. doi:10.1016/j.epsl.2018.12.028

Foster, L. C., Pearson, E. J., Juggins, S., Hodgson, D. A., Saunders, K. M., Verleyen, E., et al. (2016). Development of a regional glycerol dialkyl glycerol tetraether (GDGT)-temperature calibration for Antarctic and sub-Antarctic lakes. *Earth Planet. Sci. Lett.* 433, 370–379. doi:10.1016/j.epsl.2015.11.018

Grootes, P. M., Stuiver, M., White, J. W. C., Johnsen, S., and Jouzel, J. (1993). Comparison of oxygen isotope records from the GISP2 and GRIP Greenland ice cores. *Nature* 366, 552–554. doi:10.1038/366552a0

Günther, F., Thiele, A., Gleixner, G., Xu, B. Q., Yao, T. D., and Schouten, S. (2014). Distribution of bacterial and archaeal ether lipids in soils and surface sediments of Tibetan lakes: implications for GDGT-based proxies in saline high mountain lakes. *Org. Geochem.* 67, 19–30. doi:10.1016/j.orggeochem.2013.11.014

Günther, F., Witt, R., Schouten, S., Mäusbacher, R., Daut, G., Zhu, L., et al. (2015). Quaternary ecological responses and impacts of the Indian Ocean summer monsoon at Nam Co, Southern Tibetan Plateau. *Quat. Sci. Rev.* 112, 66–77. doi:10.1016/j.quascirev.2015.01.023

Gupta, A. K., Mohan, K., Sarkar, S., Clemens, S. C., Ravindra, R., and Uttam, R. K. (2011). East–West similarities and differences in the surface and deep northern Arabian Sea records during the past 21 Kyr. *Palaeogeogr. Palaeoclimatol. Palaeoecol.* 301, 75–85. doi:10.1016/j.palaeo.2010.12.027.

Haug, G. H., Hughen, K. A., Sigman, D. M., Peterson, L. C., and Rohl, U. (2001). Southward migration of the intertropical convergence zone through the Holocene. *Science* 293, 1304–1308. doi:10.1126/science.1059725.

He, Y., Hou, J., Brown, E. T., Xie, S., and Bao, Z. (2017). Timing of the Indian summer monsoon onset during the early Holocene: evidence from a sediment core at Linggo Co, central Tibetan plateau. *Holocene* 28, 755–766. doi:10.1177/0959683617744267.

Herzschuh, U. (2006). Palaeo-moisture evolution in monsoonal Central Asia during the last 50,000 years. *Quat. Sci. Rev.* 25, 163–178. doi:10.1016/j.quascirev.2005.02.006.

Herzschuh, U., Winter, K., Wünnemann, B., and Li, S. (2006). A general cooling trend on the central Tibetan Plateau throughout the Holocene recorded by the Lake Zigetang pollen spectra. *Quat. Int.* 154–155, 113–121. doi:10.1016/j.quaint.2006.02.005

Hopmans, E. C., Weijers, J. W. H., Schefuss, E., Herfort, L., Sinninghe Damsté, J. S., and Schouten, S. (2004). A novel proxy for terrestrial organic matter in sediments based on branched and isoprenoid tetraether lipids. *Earth Planet. Sci. Lett.* 224, 107–116. doi:10.1016/j.epsl.2004.05.012.

Hou, J., D'Andrea, W. J., and Huang, Y. (2008). Can sedimentary leaf waxes record D/H ratios of continental precipitation? Field, model, and experimental

assessments. *Geochim. Cosmochim. Acta* 72, 3503–3517. doi:10.1016/j.gca.2008.04.030.

Hou, J., D'Andrea, W. J., Wang, M., He, Y., and Liang, J. (2017). Influence of the Indian monsoon and the subtropical jet on climate change on the Tibetan Plateau since the late Pleistocene. *Quat. Sci. Rev.* 163, 84–94. doi:10.1016/j.quascirev.2017.03.013.

Hou, J., Huang, Y., Zhao, J., Liu, Z., Colman, S., and An, Z. (2016). Large Holocene summer temperature oscillations and impact on the peopling of the northeastern Tibetan Plateau. *Geophys. Res. Lett.* 43, 1323–1330. doi:10.1002/2015gl067317.

Hou, J., Li, C.-G., and Lee, S. (2019). The temperature record of the Holocene: progress and controversies. *Sci. Bull.* 64, 565–568. doi:10.1016/j.scib.2019.02.012.

Immerzeel, W. W., Lutz, A. F., Andrade, M., Bahl, A., Biemans, H., Bolch, T., et al. (2020). Importance and vulnerability of the world's water towers. *Nature* 577, 364–369. doi:10.1038/s41586-019-1822-y.

Jacob, T., Wahr, J., Pfeffer, W. T., and Swenson, S. (2012). Recent contributions of glaciers and ice caps to sea level rise. *Nature* 482, 514–518. doi:10.1038/nature10847

Jiang, D., Yu, G., Zhao, P., Chen, X., Liu, J., Liu, X., et al. (2015). Paleoclimate modeling in China: a review. *Adv. Atmos. Sci.* 32, 250–275. doi:10.1007/s00376-014-0002-0.

Kääb, A., Leinss, S., Gilbert, A., Bühler, Y., Gascoin, S., Evans, S. G., et al. (2018). Massive collapse of two glaciers in western Tibet in 2016 after surge-like instability. *Nat. Geosci.* 11, 114–120. doi:10.1038/s41561-017-0039-7.

Kaufman, D., McKay, N., Routson, C., Erb, M., Davis, B., Heiri, O., et al. (2020). A global database of Holocene paleotemperature records. *Sci. Data* 7, 115. doi:10.1038/s41597-020-0445-3.

Kim, J.-H., Schouten, S., Hopmans, E. C., Donner, B., and Sinninghe Damsté, J. S. (2008). Global sediment core-top calibration of the TEX86 paleothermometer in the ocean. *Geochim. Cosmochim. Acta* 72, 1154–1173. doi:10.1016/i.gca.2007.12.010.

Kim, J.-H., van der Meer, J., Schouten, S., Helmke, P., Willmott, V., Sangiorgi, F., et al. (2010). New indices and calibrations derived from the distribution of crenarchaeal isoprenoid tetraether lipids: implications for past sea surface temperature reconstructions. *Geochim. Cosmochim. Acta* 74, 4639–4654. doi:10.1016/j.gca.2010.05.027.

Kurt, L., Hélène, R., Anthony, P., Yiying, S., and Malcolm, S. (2014). Sea level and global ice volumes from the Last glacial maximum to the Holocene. *Proc. Natl. Acad. Sci. U.S.A.* 111, 15296–15303.

Kutzbach, J., Guetter, P. J., Behling, P., and Selin, R. (1993). "Simulated climatic changes: results of the COHMAP climate-model experiments," in *Global climates since the Last Glacial Maximum*. Editors H. E. Wright, Jr, J. E. Kutzbach, T. Webb, III, W. F. Ruddiman, F. A. Street-Perrott, and P. J. Bartlein (Minneapolis, MN: University of Minnesota Press), 24–93.

Lei, Y. B., Yao, T. D., Yi, C. L., Wang, W. C., Sheng, Y. W., Li, J., et al. (2012). Glacier mass loss induced the rapid growth of Linggo Co on the central Tibetan Plateau. *J. Glaciol.* 58, 177–184. doi:10.3189/2012JoG11J025.

Li, M. S., Babel, W., Chen, X., Zhang, L., Sun, F., Wang, B., Ma, Y., Hu, Z., and Foken, T. (2015). A 3-year dataset of sensible and latent heat fluxes from the Tibetan Plateau, derived using eddy covariance measurements. *Theor. Appl. Climatol.* 122, 457–469. doi:10.1007/s00704-014-1302-0

Li, X. M., Wang, M. D., Zhang, Y. Z., Lei, L., and Hou, J. Z. (2017). Holocene climatic and environmental change on the western Tibetan Plateau revealed by glycerol dialkyl glycerol tetraethers and leaf wax deuterium-to-hydrogen ratios at Aweng Co. *Quat. Res.* 87, 455–467. doi:10.1017/qua.2017.9.

Li, X. Z., Yi, C. L., Chen, F. H., Yao, T. D., and Li, X. (2006). Formation of proglacial dunes in front of the Puruogangri Icefield in the central Qinghai-Tibet Plateau: implications for reconstructing paleoenvironmental changes since the Lateglacial. *Quat. Int.* 154–155, 122–127. doi:10.1016/j.quaint.2006.02.006.

Lin, Y., Ramstein, G., Wu, H., Rani, R., Braconnot, P., Kageyama, et al. (2019). Mid-Holocene climate change over China: model-data discrepancy. *Clim. Past.* 15, 1223–1249. doi:10.5194/cp-15-1223-2019.

Liu, X., Cheng, Z., Yan, L., and Yin, Z.-Y. (2009). Elevation dependency of recent and future minimum surface air temperature trends in the Tibetan Plateau and its surroundings. *Global Planet. Change* 68, 164–174. doi:10.1016/j.gloplacha.2009.03.017

Liu, X. J., Colman, S., Brown, E., An, Z. S., Zhou, W. J., Jull, A. J., et al. (2014). A climate threshold at the eastern edge of the Tibetan Plateau. *Geophys. Res. Lett.* 41, 5589–5604. doi:10.1002/2014GL060833.

Liu, Z., Zhu, J., Rosenthal, Y., Zhang, X., Otto-Bliesner, B. L., Timmermann, A., et al. (2014). The Holocene temperature conundrum. *Proc. Natl. Acad. Sci. U.S.A.* 111, E3501–E3505. doi:10.1073/pnas.1407229111.

Loomis, S. E., Russell, J. M., Heureux, A. M., D'Andrea, W. J., and Sinninghe Damsté, J. S. (2014). Seasonal variability of branched glycerol dialkyl glycerol tetraethers (brGDGTs) in a temperate lake system. *Geochim. Cosmochim. Acta* 144, 173–187. doi:10.1016/j.gca.2014.08.027.

Lu, H. X., Liu, W. G., Yang, H., Wang, H. Y., Liu, Z. H., Leng, Q., et al. (2019). 800-kyr land temperature variations modulated by vegetation changes on Chinese Loess Plateau. *Nat. Commun.* 10, 1958. doi:10.1038/s41467-019-09978-1.

Lu, H. Y., Wu, N. Q., Liu, K.-b., Zhu, L. P., Yang, X. D., Yao, T. D., et al. (2011). Modern pollen distributions in Qinghai-Tibetan Plateau and the development of transfer functions for reconstructing Holocene environmental changes. *Quat. Sci. Rev.* 30, 947–966. doi:10.1016/j.quascirev.2011.01.008.

Lundeen, Z. J., and Brunelle, A. (2016). A 14,000-year record of fire, climate, and vegetation from the Bear River Range, southeast Idaho, United States. *Holocene* 26, 833–842. doi:10.1177/0959683615622545.

Ma, Q., Zhu, L., Lü, X., Guo, Y., Ju, J., Wang, J., et al. (2014). Pollen-inferred Holocene vegetation and climate histories in Taro Co, southwestern Tibetan Plateau. *Chin. Sci. Bull.* 59, 4101–4114. doi:10.1007/s11434-014-0505-1

Ma, N., Zhang, Y., Guo, Y., Gao, H., Zhang, H., and Wang, Y. (2015). Environmental and biophysical controls on the evapotranspiration over the highest alpine steppe. *J. Hydrol.* 529, 980–992. doi:10.1016/j.jhydrol.2015.09.013.

Magny, M., Combourieu-Nebout, N., de Beaulieu, J. L., Bout-Roumazeilles, V., Colombaroli, D., Desprat, S., et al. (2013). North-south palaeohydrological contrasts in the central Mediterranean during the Holocene: tentative synthesis and working hypotheses. *Clim. Past.* 9, 2043–2071. doi:10.5194/cp-9-2043-2013.

Marcott, S. A., Shakun, J. D., Clark, P. U., and Mix, A. C. (2013). A reconstruction of regional and global temperature for the past 11,300 years. *Science* 339, 1198–1201. doi:10.1126/science.1228026.

Marsicek, J., Shuman, B. N., Bartlein, P. J., Shafer, S. L., and Brewer, S. (2018). Reconciling divergent trends and millennial variations in Holocene temperatures. *Nature* 554, 92–96. doi:10.1038/nature25464

Naafs, B. D. A., Inglis, G. N., Zheng, Y., Amesbury, M. J., Biester, H., Bindler, R., et al. (2017). Introducing global peat-specific temperature and pH calibrations based on brGDGT bacterial lipids. *Geochim. Cosmochim. Acta* 208, 285–301. doi:10.1016/j.gca.2017.01.038.

Neckel, N., Kropáček, J., Bolch, T., and Hochschild, V. (2014). Glacier mass changes on the Tibetan Plateau 2003–2009 derived from ICESat laser altimetry measurements. *Environ. Res. Lett.* 9, 014009. doi:10.1088/1748-9326/9/1/014009.

Pan, B. L., Yi, C. L., Jiang, T., Dong, G. C., Hu, G., and Jin, Y. (2012). Holocene lake-level changes of Linggo Co in central Tibet. *Quat. Geochronol.* 10, 117–122. doi:10.1016/j.quageo.2012.03.009.

Park, H.-S., Kim, S.-J., Stewart, A. L., Son, S.-W., and Seo, K.-H. (2019). Mid-holocene Northern hemisphere warming driven by Arctic amplification. *Sci. Adv.* 5, eaax8203. doi:10.1126/sciadv.aax8203.

Pearson, E. J., Juggins, S., Talbot, H. M., Weckström, J., Rosén, P., Ryves, D. B., et al. (2011). A lacustrine GDGT-temperature calibration from the Scandinavian Arctic to Antarctic: renewed potential for the application of GDGT-paleothermometry in lakes. *Geochim. Cosmochim. Acta* 75, 6225–6238. doi:10.1016/j.gca.2011.07.042.

Peterse, F., van der Meer, J., Schouten, S., Weijers, J. W. H., Fierer, N., Jackson, R. B., et al. (2012). Revised calibration of the MBT–CBT paleotemperature proxy based on branched tetraether membrane lipids in surface soils. *Geochim. Cosmochim. Acta* 96, 215–229. doi:10.1016/j.gca.2012.08.011.

Powers, L. A., Werne, J. P., Johnson, T. C., Hopmans, E. C., Sinninghe Damsté, J. S., and Schouten, S. (2004). Crenarchaeotal membrane lipids in lake sediments: a new paleotemperature proxy for continental paleoclimate reconstruction? *Geology* 32, 613–616. doi:10.1130/g20434.1.

Powers, L., Werne, J. P., Vanderwoude, A. J., Sinninghe Damsté, J. S., Hopmans, E. C., et al. (2010). Applicability and calibration of the TEX86 paleothermometer in lakes. *Org. Geochem.* 41, 404–413. doi:10.1016/j.orggeochem.2009.11.009.

Qiu, J. (2008). China: the third pole. *Nature* 454, 393–396. doi:10.1130/B26043.1

Renssen, H., Seppä, H., Heiri, O., Roche, D. M., Goosse, H., and Fichefet, T. (2009). The spatial and temporal complexity of the Holocene thermal maximum. *Nat. Geosci.* 2, 411–414. doi:10.1038/ngeo513

Russell, J. M., Hopmans, E. C., Loomis, S. E., Liang, J., and Sinninghe Damsté, J. S. (2018). Distributions of 5- and 6-methyl branched glycerol dialkyl glycerol

tetraethers (brGDGTs) in East African lake sediment: effects of temperature, pH, and new lacustrine paleotemperature calibrations. *Org. Geochem.* 117, 56–69. doi:10.1016/j.orggeochem.2017.12.003.

Sachse, D., Billault, I., Bowen, G. J., Chikaraishi, Y., Dawson, T. E., Feakins, S. J., et al. (2012). Molecular paleohydrology: interpreting the hydrogen-isotopic composition of Lipid biomarkers from photosynthesizing organisms. *Annu. Rev. Earth Planet. Sci.* 40, 221–249. doi:10.1146/annurev-earth-042711-105535.

Sachse, D., Radke, J., and Gleixner, G. (2004). Hydrogen isotope ratios of recent lacustrine sedimentary n-alkanes record modern climate variability. *Geochim. Cosmochim. Acta* 68, 4877–4889. doi:10.1016/j.gca.2004.06.004.

Sachse, D., Radke, J., and Gleixner, G. (2006). δD values of individual n-alkanes from terrestrial plants along a climatic gradient—Implications for the sedimentary biomarker record. *Org. Geochem.* 37, 469–483. doi:10.1016/j.orggeochem.2005.12.003.

Schneider, B., Leduc, G., and Park, W. (2010). Disentangling seasonal signals in Holocene climate trends by satellite-model-proxy integration. *Paleoceanography* 25, PA4217. doi:10.1029/2009PA001893.

Schneider, T., Bischoff, T., and Haug, G. H. (2014). Migrations and dynamics of the intertropical convergence zone. *Nature* 513, 45–53. doi:10.1038/nature13636.

Schouten, S., Eldrett, J., Greenwood, D. R., Harding, I., Baas, M., and Damsté, J. S. S. (2008). Onset of long-term cooling of Greenland near the Eocene-Oligocene boundary as revealed by branched tetraether lipids. *Geology* 36, 147–150. doi:10.1130/G24332a.1.

Schouten, S., Forster, A., Panoto, F. E., and Sinninghe Damsté, J. S. (2007). Towards calibration of the TEX86 palaeothermometer for tropical sea surface temperatures in ancient greenhouse worlds. *Org. Geochem.* 38, 1537–1546. doi:10.1016/j.orggeochem.2007.05.014.

Schouten, S., Hopmans, E. C., Schefuss, E., and Sinninghe Damsté, J. S. (2002). Distributional variations in marine crenarchaeotal membrane lipids: a new tool for reconstructing ancient sea water temperatures? *Earth Planet. Sci. Lett.* 204, 265–274. doi:10.1016/s0012-821x(02)00979-2

Schouten, S., Hopmans, E. C., and Sinninghe Damsté, J. S. (2013). The organic geochemistry of glycerol dialkyl glycerol tetraether lipids: a review. *Org. Geochem.* 54, 19–61. doi:10.1016/j.orggeochem.2012.09.006

Shakun, J. D., Clark, P. U., He, F., Marcott, S. A., Mix, A. C., Liu, Z., et al. (2012). Global warming preceded by increasing carbon dioxide concentrations during the last deglaciation. *Nature* 484, 49–54. doi:10.1038/nature10915

Shi, Q., and Liang, S. (2014). Surface-sensible and latent heat fluxes over the Tibetan Plateau from ground measurements, reanalysis, and satellite data. *Atmos. Chem. Phys.* 14, 5659–5677. doi:10.5194/acp-14-5659-2014

Sinninghe Damsté, J. S. (2016). Spatial heterogeneity of sources of branched tetraethers in shelf systems: the geochemistry of tetraethers in the Berau River delta (Kalimantan, Indonesia). *Geochim. Cosmochim. Acta* 186, 13–31. doi:10.1016/j.gca.2016.04.033.

Sinninghe Damsté, J. S., Ossebaar, J., Abbas, B., Schouten, S., and Verschuren, D. (2009). Fluxes and distribution of tetraether lipids in an equatorial African lake: constraints on the application of the TEX86 palaeothermometer and BIT index in lacustrine settings. *Geochim. Cosmochim. Acta* 73, 4232–4249. doi:10.1016/j.gca.2009.04.022.

Sinninghe Damsté, J. S., Rijpstra, W. I. C., Hopmans, E. C., Prahl, F. G., Wakeham, S. G., and Schouten, S. (2012). Distribution of membrane Lipids of planktonic crenarchaeota in the Arabian Sea. *Appl. Environ. Microbiol.* 68, 2997–3002.

Stuiver, M., and Grootes, P. M. (2000). GISP2 oxygen isotope ratios. *Quat. Res.* 53, 277–284. doi:10.1006/qres.2000.2127.

Sun, Q., Chu, G., Liu, M., Xie, M., Li, S., Ling, Y., et al. (2011). Distributions and temperature dependence of branched glycerol dialkyl glycerol tetraethers in recent lacustrine sediments from China and Nepal. *J. Geophys. Res.* 116, G01008. doi:10.1029/2010JG001365.

Thompson, L. G., Tandong, Y., Davis, M. E., Mosley-Thompson, E., Mashiotta, T. A., Lin, P.-N., et al. (2006). Holocene climate variability archived in the Puruogangri ice cap on the central Tibetan Plateau. *Ann. Glaciol.* 43, 61–69. doi:10.3189/172756406781812357

Tian, L. D., Yao, T. D., MacClune, K., White, J. W. C., Schilla, A., Vaughn, B., et al. (2007). Stable isotopic variations in west China: a consideration of moisture sources. *J. Geophys. Res.* 112, D10112. doi:10.1029/2006jd007718.

Tierney, J. E., and Russell, J. M. (2009). Distributions of branched GDGTs in a tropical lake system: implications for lacustrine application of the MBT/CBT paleoproxy. *Org. Geochem.* 40, 1032–1036. doi:10.1016/j.orggeochem.2009.04.014.

Veh, G., Korup, O., and Walz, A. (2020). Hazard from Himalayan glacier lake outburst floods. *Proc. Natl. Acad. Sci. US.A.* 117, 907–912. doi:10.1073/pnas.1914898117.

Wang, Y. B., Liu, X. Q., and Herzschuh, U. (2010). Asynchronous evolution of the Indian and East Asian summer monsoon indicated by Holocene moisture patterns in monsoonal central Asia. *Earth-Sci. Rev.* 103, 135–153. doi:10.1016/j.earscirev.2010.09.004.

Wang, H., Liu, W., Zhang, C. L., Wang, Z., Wang, J., Liu, Z., et al. (2012). Distribution of glycerol dialkyl glycerol tetraethers in surface sediments of Lake Qinghai and surrounding soil. *Org. Geochem.* 47, 78–87. doi:10.1016/j.orggeochem.2012.03.008.

Wang, M., Hou, J., and Lei, Y. (2014). Classification of Tibetan lakes based on variations in seasonal lake water temperature. *Chin. Sci. Bull.* 59, 4847–4855. doi:10.1007/s11434-014-0588-8.

Wang, M. D., Liang, J., Hou, J. Z., and Hu, L. (2016). Distribution of GDGTs in lake surface sediments on the Tibetan Plateau and its influencing factors. *Sci. China Earth Sci.* 59, 961–974. doi:10.1007/s11430-015-5214-3.

Wang, H., Dong, H., Zhang, C. L., Jiang, H., Liu, Z., Zhao, M., et al. (2015). Deglacial and holocene archaeal lipid-inferred paleohydrology and paleotemperature history of Lake Qinghai, Northeastern Qinghai-Tibetan Plateau. *Quat. Res.* 83, 116–126. doi:10.1016/j.yqres.2014.10.003.

Wang, Z., Liu, Z., Zhang, F., Fu, M., and An, Z. (2015). A new approach for reconstructing Holocene temperatures from a multi-species long chain alkenone record from Lake Qinghai on the northeastern Tibetan Plateau. *Org. Geochem.* 88, 50–58. doi:10.1016/j.orggeochem.2015.08.006.

Warden, L., Kim, J.-H., Zell, C., Vis, G.-J., de Stigter, H., Bonnin, J., et al. (2016). Examining the provenance of branched GDGTs in the Tagus River drainage basin and its outflow into the Atlantic Ocean over the Holocene to determine their usefulness for paleoclimate applications. *Biogeosciences* 13, 5719–5738. doi:10.5194/bg-13-5719-2016.

Weijers, J. W. H., Bernhardt, B., Peterse, F., Werne, J. P., Dungait, J. A. J., Schouten, S., et al. (2011). Absence of seasonal patterns in MBT-CBT indices in mid-latitude soils. *Geochim. Cosmochim. Acta* 75, 3179–3190. doi:10.1016/j.gca.2011.03.015.

Weijers, J. W. H., Schefuss, E., Schouten, S., and Damste, J. S. S. (2007a). Coupled thermal and hydrological evolution of tropical Africa over the last deglaciation. *Science* 315, 1701–1704. doi:10.1126/science.1138131.

Weijers, J. W. H., Schouten, S., van den Donker, J. C., Hopmans, E. C., and Sinninghe Damsté, J. S. (2007b). Environmental controls on bacterial tetraether membrane lipid distribution in soils. *Geochim. Cosmochim. Acta* 71, 703–713. doi:10.1016/j.gca.2006.10.003.

Weijers, J. W. H., Schouten, S., Hopmans, E. C., Geenevasen, J. A. J., David, O. R. P., Coleman, J. M., et al. (2006). Membrane lipids of mesophilic anaerobic bacteria thriving in peats have typical archaeal traits. *Environ. Microbiol.* 8, 648–657. doi:10.1111/j.1462-2920.2005.00941.x.

Wuchter, C., Schouten, S., Coolen, M. J. L., and Sinninghe Damsté, J. S. (2004). Temperature-dependent variation in the distribution of tetraether membrane lipids of marine Crenarchaeota: implications for TEX86paleothermometry. *Paleoceanography* 19, 4. doi:10.1029/2004pa001041.

Yang, G., Zhang, C. L., Xie, S., Chen, Z., Gao, M., Ge, Z., et al. (2013). Microbial glycerol dialkyl glycerol tetraethers from river water and soil near the Three Gorges Dam on the Yangtze River. *Org. Geochem.* 56, 40–50. doi:10.1016/j.orggeochem.2012.11.014

Yao, T., Masson-Delmotte, V., Gao, J., Yu, W., Yang, X., Risi, C., et al. (2013). A review of climatic controls on δ18O in precipitation over the Tibetan Plateau: observations and simulations. *Rev. Geophys.* 51, 525–524. doi:10.1002/rog.20023.

Yao, T., Xue, Y., Chen, D., Chen, F., Thompson, L., Cui, P., et al. (2019). Recent third pole's rapid warming accompanies cryospheric melt and water cycle intensification and interactions between monsoon and environment: multidisciplinary approach with observations, modelling, and analysis. *Bull. Am. Meteorol. Soc.* 100, 423–447. doi:10.1175/BAMS-D-17-0057.1.

Yao, T. D., Thompson, L., Yang, W., Yu, W. S., Gao, Y., Guo, X. J., et al. (2012). Different glacier status with atmospheric circulations in Tibetan Plateau and surroundings. *Nat. Clim. Change* 2, 663–667. doi:10.1038/Nclimate1580.

Zell, C., Kim, J.-H., Moreira-Turcq, P., Abril, G. L., Hopmans, E. C., Bonnet, M.-P., et al. (2013). Disentangling the origins of branched tetraether lipids and crenarchaeol in the lower Amazon River: implications for GDGT-based proxies. *Limnol. Oceanogr.* 58, 343–353. doi:10.4319/lo.2013.58.1.0343

Zhang, C. L., Liu, X. L., Li, L., Hinrichs, K.-U., and Noakes, J. E. (2011). Methane index: a tetraether archaeal lipid biomarker indicator for detecting the instability of marine gas hydrates. *Earth Planet Sci. Lett.* 307, 525–534.

Zhao, J. J., An, C.-B., Huang, Y., Morrill, C., and Chen, F.-H. (2017). Contrasting early Holocene temperature variations between monsoonal East Asia and westerly dominated Central Asia. *Quat. Sci. Rev.* 178, 14–23. doi:10.1016/j.quascirev.2017.10.036.

Zhu, C., Weijers, J. W. H., Wagner, T., Pan, J.-M., Chen, J.-F., and Pancost, R. D. (2011). Sources and distributions of tetraether lipids in surface sediments across a large river-dominated continental margin. *Org. Geochem.* 42, 376–386. doi:10.1016/j.orggeochem.2011.02.002

Zhu, L., Wang, J., Ju, J., Zhang, Y., Liu, C., Han, B., et al. (2019). Climatic and lake environmental changes in the Serling Co region of Tibet over a variety of timescales. *Sci. Bull.* 64, 10–12. doi:10.1016/j.scib.2019.02.016

Conflict of Interest: The authors declare that the research was conducted in the absence of any commercial or financial relationships that could be construed as a potential conflict of interest.